

CL – 08/118/CES

**INVESTIGATION OF CYCLING-INDUCED
PERFORMANCE DEGRADATION OF SODIUM
ALANATES**

DANIEL DEDRICK
Sandia National Laboratories

ROBERT D. STEPHENS
Chemical and Environmental Sciences Laboratory

Approved by Mei Cai, Lab Group Manager
Approved by James A. Spearot, Lab Director
Chemical and Environmental Sciences Laboratory



COLLABORATIVE REPORT

GM RESEARCH & DEVELOPMENT CENTER

September 15, 2008

Abstract

Samples of NaAlH_4 with 18 weight percent excess aluminum and catalyzed with 3 mole percent of TiCl_3 were aged for up to 100 absorption and desorption cycles while monitoring the hydrogen uptake capacity and rate of absorption. The sample demonstrated significant decreases in uptake capacity during the aging process, decreasing from a 10 minute hydrogen capacity of 3.4 wt% to 2.8% over the 100 cycles. Apparent kinetics were also affected adversely by cycling with rates of absorption decreasing in excess of 50%.

To determine the cause of this loss of performance, samples of the 100-cycle aged material (referred to as “aged”) were compared to samples of 10-cycle aged materials (referred to as “fresh”) utilizing a number of analytical tests. Tests and measurements were selected to highlight the differences in sample contamination content, morphology, and reactant separation. These tests included Fourier Transform Infrared Spectroscopy, aluminum neutron magnetic resonance, x-ray diffraction, scanning electron microscopy, residual gas analysis, thermal-gravimetric decomposition analysis, scanning electron microscopy, and energy dispersive X-ray spectroscopy. The hydrogen used for material cycling was tested for O_2 , H_2O , and other impurities that might have caused either oxidation or contamination of the NaAlH_4 .

The presence of aluminum oxidation or contamination was not detected by NMR or XRD. The possibility of low-level sodium contamination was observed during thermal decomposition analysis. Morphological differences were observed, specifically, the formation of an intermetallic Ti/Al alloy that is likely to be responsible for the hydrogen capacity and kinetic degradation. The formation of titanium-rich sodium clusters was observed in the aged materials. This titanium is unlikely to participate in the hydrogenation reaction as it is not in proximity to an aluminum particle.

Restoration experiments were performed by utilizing slow absorption/desorption cycles in an attempt to limit agglomeration of the reactants. These tests failed to restore 10-minute capacity of the material to its original performance. Subsequent ball milling of the 100-cycle material did restore kinetics and 10-minute absorption capacity.

Purpose of the Research

The purpose of this research was to investigate the causes for performance degradation of titanium-doped sodium alanate after repeated hydrogen cycling.

Conclusions

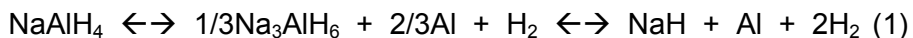
Repeated cycling of Ti-doped sodium alanate show a linear decrease in 10-minute hydrogen capacity as a function of the number of absorption/desorption cycles the material undergoes. Analyses indicated that morphological changes in the material are the likely cause in performance degradation. Some low-level sodium oxidation may occur after cycling and limit the overall reversible capacity. Material performance can be restored to near original condition by ball milling.

Significance

Capacity and kinetics of hydrogen absorption via sodium alanate decreases with repeated absorption/desorption cycling. This performance degradation is substantial, representing a 17% decrease in hydrogen capacity after 100 cycles.

Introduction

Sandia National Laboratories, under contract to General Motors, has designed and tested hydrogen storage systems based upon the equilibrium reactions of sodium alanates (NaAlH_4 , Na_3AlH_6):



The sodium alanates used for this study were catalyzed with 3 mole% of TiCl_3 through the direct synthesis process. Also, prior testing at Sandia has confirmed that absorption capacities attained after short absorption times, e.g. 10 minutes, can be enhanced by adding extra aluminum, despite the decrease in overall total capacity that can be reached by this effective dilution of the NaAlH_4 . Other benefits of adding excess aluminum have been reported by Bogdanovic et al.¹ Consequently, the alanate used in these tests also had 18 weight% excess aluminum over the stoichiometric amount needed for the reaction from right to left in reaction (1).

In vehicular applications, reaction (1) from left to right can be used to provide fuel for a hydrogen powered vehicle. Vehicle refueling takes place by the reverse reaction, i.e. reaction (1) from right to left. This reversible reaction must occur many times throughout the life of a vehicle. For example, if reaction (1) provides enough hydrogen to power a vehicle for 300 miles and the vehicle lifetime is 150,000 miles, reaction (1) must cycle 500 times. Consequently, the ability of sodium alanate to repeatedly cycle is of great importance if it is to be used for on-board vehicular storage of hydrogen fuel.

In this study, the formulation of sodium alanate described above was subjected to 10 and 100 absorption/desorption cycles to determine material performance as a function of age. H_2 absorption capacity measured at 10 minutes into the absorption showed significant degradation as a function of cycle number. Decreased capacity after repeated hydrogen cycling has also been observed by Srinivasan et al.² The sodium alanate that was underwent 100 cycles was subjected to a battery of analytical tests to understand the causes for kinetic and absorption capacity degradation.

In this report, the “capacity” is relative rather than absolute term that refers to the hydrogen uptake resulting from either a 10 or 30 minute exposure to 122 bar hydrogen pressure and 150 °C temperature. Similarly, the term “kinetics” is a relative term referring to the average rate of hydrogen uptake.

Experimental Methods

Preparation of the sodium alanate samples followed a two step process. First, the NaH, Al, and TiCl_3 were mixed in a Fristch P5 ball mill at 280 rpm for three 60 minute milling, 90 minute cooling cycles with rotation reversal. Two 20 gram samples were then loaded into vessels and cycled in parallel. Kinetics and capacity were compared for the two samples after 7 cycles to verify sample continuity. Typical absorptions were performed at 140 - 155 °C and 122 bar of hydrogen pressure for 30 minutes with Ultra High Purity (UHP) hydrogen gas from Matheson Tri-Gas. Typical desorptions were performed with a thermal ramp from 150 to 200 °C with desorption pressures maintained under a maximum of 3 bar for 60 minutes. For the purposes of this report, the samples will be designated as “fresh” in the case of the 10-cycle sample, and “aged” for the 100-cycle sample.

After aging was completed, small samples were extracted from the absorption/desorption vessels while leaving the bulk of each sample intact. The small samples extracted from the vessels were used for various analytical tests used in an attempt to understand the causes for material performance degradation.

For Al NMR tests, both fresh and aged sodium alanate samples were separately loaded into clean ZrO_2 rotors inside of a glovebox and sealed with Kel F endcaps. Solid state ^{27}Al NMR MAS experiments were performed on a Bruker Avance 400 MHz NMR spectrometer with a ^{27}Al Lamor frequency of 104.3 MHz. The samples were loaded into 4 mm ZrO_2 rotors inside a glove box and spun at 10 kHz after transferring to the probe. The spectra were collected using a 2.5 μs pulse width (single pulse sequence), an acquisition time of 2.46 ms, and a relaxation delay of 5 seconds between pulses. As many as 8000 scans were collected to obtain high signal to noise spectra. An unusually large spectral width of 4078 ppm was employed in order to capture the Knight-shifted signal of the Al metal present in the samples.

For FTIR spectra, fresh and aged samples of the sodium alanate were ground in a mortar and pestle with KBr inside of a glovebox. Pellets made in this fashion were then pressed and sealed between 2 KBr discs separated by a rubber o-ring. Transmission spectra were obtained on Nicolet Magna-IR 760 spectrometer equipped with a room temperature DTGS detector. Thirty two scans were signal averaged at a resolution of 4 cm^{-1} for each sample.

For crystallographic comparisons, XRD spectra were obtained with a theta 2-theta Scintag XDS 2000 powder diffractometer.

Thermogravimetric type measurements were made with a Simultaneous Thermo-gravimetric Modulated-Beam Mass Spectrometer³. Small samples are placed in a mass effusion cell and are loaded in a tube furnace and mounted on a micro-balance. The sample is thermally decomposed at

temperatures up to 1000 °C. The typical data collected are the mass spectra of the gaseous species evolving from the sample and the mass loss of the sample as a function of time during the course of a heating experiment. A combination of the mass loss data and mass spectra are then analyzed to provide the identities and partial pressures of each gaseous species within the reaction cell as a function of time. This information can then be used to determine vapor pressures and rates of decomposition. Additionally this tool can be utilized to detect the decomposition of volatile contaminating species such as water vapor from hydrates.

Gas Analysis was conducted by Atlantic Analytic Laboratory using a GC/IR analysis method.

Results

A plot of the absorption capacity as a function of absorption/desorption cycle is shown in **Figure 1**. The two data sets represent the hydrogen capacities measured after 10 minutes and 30 minutes of exposure to hydrogen at 155 °C and 122 bar. The slope of the capacities as a function of cycle number indicate that the 10-minute capacities degrade more rapidly than the 30-minute capacities. This demonstrates a reduction in kinetics as well as capacity as shown in a comparison of fresh, aged, and remilled absorption profiles as shown in **Figure 2**. The re-milling process will be explored further in the *Results* section below. The linear regression best fit to the 10-minute absorption data indicate that the capacity decrease over 100 cycles is 0.58 weight%, a 17% relative decrease from the capacity of the material after 10 absorption/desorption cycles.

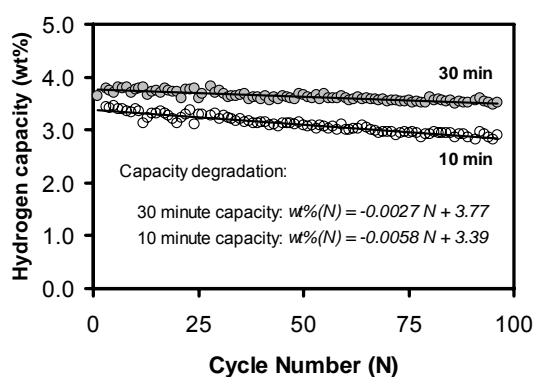


Figure 1. Absorption capacities measured after 10-minute and 30-minute absorption times. Absorption conditions were 155 °C and 122 bar hydrogen overpressure.

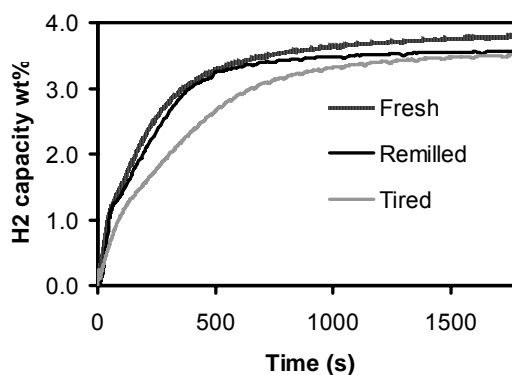


Figure 2. Relative kinetic and capacity comparison for fresh, aged, and remilled samples undergoing 30 minute absorptions at 122 bar and 150 °C

This absorption degradation can be attributed to a number of possible causes as follow:

- 1) Sample contamination with organic material entrained in the H₂ stream
- 2) Oxidation of the alanate from O₂ and/or H₂O entrained in the H₂ stream
- 3) Morphological changes in the material that reduces the reactive surface area of the solid reacting species
- 4) A decrease in catalytic activity due to changes in the titanium catalyst

To better understand potential causes of the degradation in performance, the total hydrogen capacities of each phase of each material was measured. To accomplish this, the completely dehydrogenated 100-cycle material (aged) was first hydrogenated under temperature and pressure conditions that thermodynamically limit the absorption to the hexahydride phase (Na₃AlH₆). That material was then further hydrogenated fully to the tetrahydride phase (NaAlH₄) until equilibrium was attained. Similar absorption tests were conducted on material that had been subjected to only 10 absorption/desorption cycles. These test results shown in **Table I** indicate that both alanate phases of the aged material showed nearly a 10% reduction of the full capacity relative to that observed for the fresh material. Hence, the performance degradation over 100-cycles is not phase dependent. After re-milling the aged material, the hexahydride capacity was fully restored. The tetrahydride kinetics were restored and the capacity recovered to within 0.17 wt% of the fresh material.

A series of tests were conducted to detect material contamination. The hydrogen used for cycling the alanate was tested for purity. Results of these tests are shown in **Table II**. The hydrogen had undetectable levels of hydrocarbons, 5.6 ppm of H₂O, and 1.3 ppm levels of O₂. In theory, these water and oxygen levels should be insufficient to result in significant oxidation of the aged sodium alanate depending on assumptions for exposure time.

To investigate the presence of hydrocarbon or oxidation contamination in the aged sample, thermogravimetric decomposition, Al-NMR spectra, and Fourier Transform Infrared Spectra were taken of the fresh and aged materials.

Thermogravimetric measurements were performed on both the fresh and aged samples at temperatures up to 1000 °C. The mass-spectrum of the gas evolving from the sample did not indicate the presence of any hydrocarbon contamination, however, the possibility of the presence of low-level sodium oxidation was identified. The decomposition of fresh samples (**Figure 3**, left) results in the evolution of 85% of the sodium during the dehydrogenation of NaH and the remainder continuing to ~650 °C. When sodium oxides are present, oxide decomposition and subsequent detection of sodium is experienced at temperatures above 700 °C as observed by previous efforts⁴. During decomposition of the aged material, 70% of the sodium evolves during dehydrogenation of NaH, similar to the fresh material; however, a new portion of Na evolves between 600 and 750°C (see arrow in **Figure 3**). The evolution of sodium in this temperature range is observed in intentionally oxidized samples⁴.

FTIR measurements were made on the fresh and aged materials to investigate the presence of hydrocarbon contamination in the samples (**Figure 4**).

Hydrocarbon C-H stretches would be expected to be observed between 3000 and 2840 cm⁻¹ (shaded region) if the material were contaminated with organic material⁵. The spectra presented here do not indicate the presence of organic material contamination.

AL-NMR spectra for the fresh and aged materials were obtained to investigate the presence of aluminum oxidation (**Figure 5**). These spectra do not indicate the presence of aluminum oxides.

The XRD spectra, as shown in **Figure 6 and Figure 7** do show subtle changes in the aged material relative to the fresh material. In particular, there are changes in the width of the line at 38.5° two-theta angle. Aluminum and sodium oxides were not apparent in the XRD spectra.

To further investigate the morphological changes, SEM/EDX measurements were made on the fresh and aged materials. SEM images indicated changes in the particle appearance (morphology) with cycling (

Table I. Comparison of actual material capacities for fresh and cycled alanate relative to theoretical capacity.

State	Total	HEX	TET
Theoretical	4.28	1.43	2.85
10 cycles	4.02	1.37	2.61
100 cycles	3.56	1.2	2.36
Re-milled	3.69	1.35	2.44

Table II. Results of H₂ purity test

Test Description (units)	Result	Detection Limit
Total Hydrocarbons (ppm)	ND	0.1
Water vapor (ppm)	5.6	0.5
Carbon monoxide (ppm)	ND	0.1
Carbon dioxide (ppm)	1.1	0.1
Acetylene (ppm)	ND	0.1
Nitrous oxide (ppm)	ND	0.1
Methane (ppm)	ND	0.1
Nitrogen (ppm)	250	0.5
Oxygen (ppm)	1.3	0.1
Argon (ppm)	25	0.5
Hydrogen (%)	99.87	--

Figure 8). Two distinct types of particles are observed in the SEM images: a “spherical” phase and a “fine cluster” phase (see **Figure 9**). The spherical phase is more prevalent in the fresh materials while the fine cluster is more likely to appear in the aged materials. Analysis using EDX capabilities of 3 μm and smaller particles indicated that the bulk properties of the spherical phase tended to be predominately aluminum with very little detectable titanium, while the fine clusters tended to be titanium rich sodium particles.

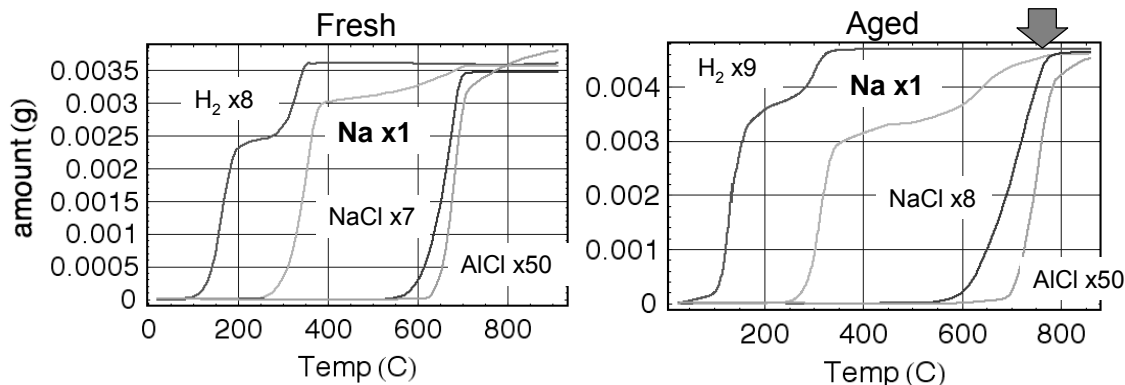


Figure 3. Decomposition product analysis indicated subtle differences in the two samples above 200 °C. Although approximately 3.4 wt% of reversible hydrogen was released from each sample, the vaporization characteristics of the sodium signal varied noticeably.

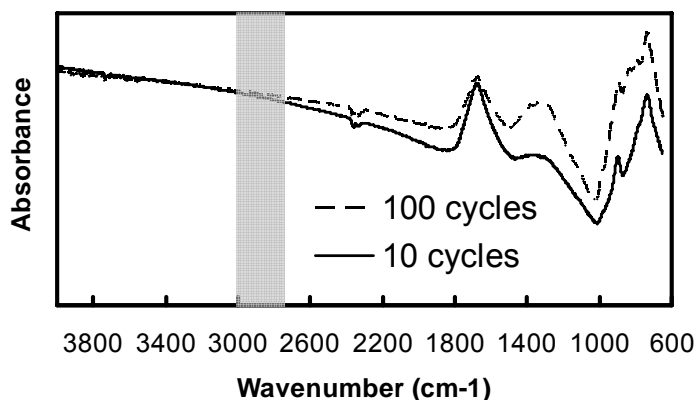


Figure 4. FTIR spectra for the 10-cycle and 100-cycle sodium alanate indicating that no C-H stretches are observed in the material.

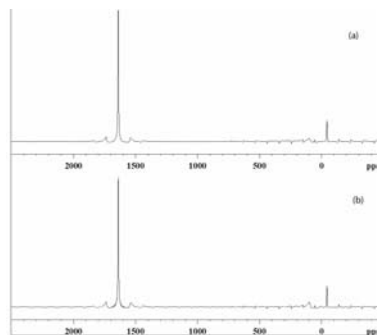


Figure 5. NMR spectra of (a) fresh and (b) aged samples of NaAlH_4 . Neither samples show any indication of aluminum oxidation, which would show at between 0 and 10 ppm.

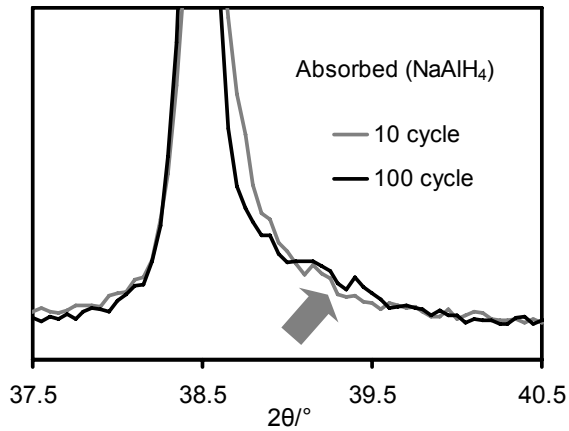


Figure 6. XRD spectra for fresh and aged fully hydrogenated sodium alanate

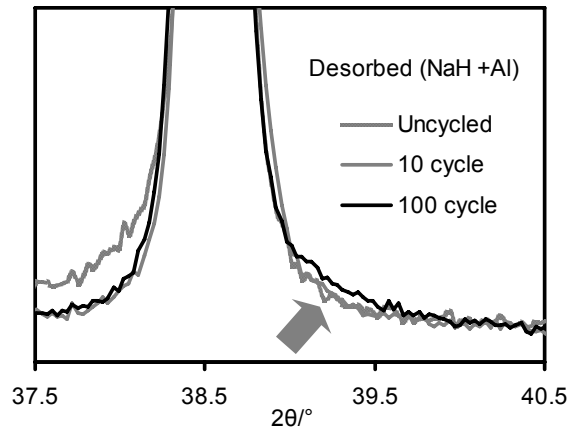


Figure 7. XRD spectra for the fresh and aged sodium alanate.

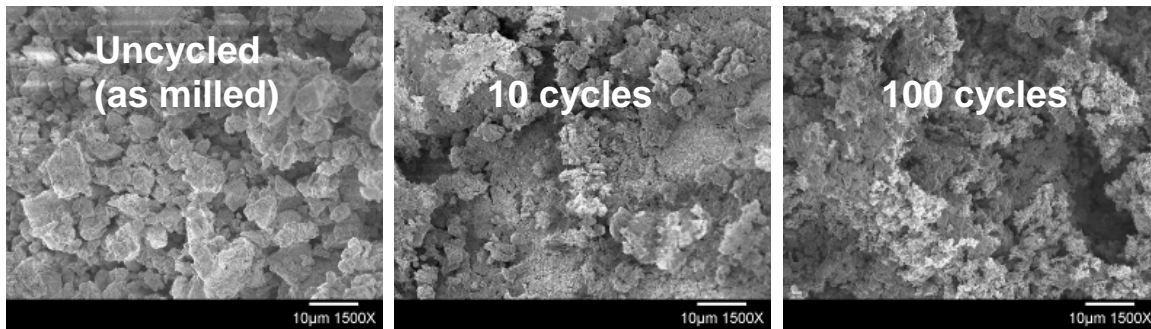


Figure 8. Apparent increase in surface area resulting from cycling was observed from SEM imaging

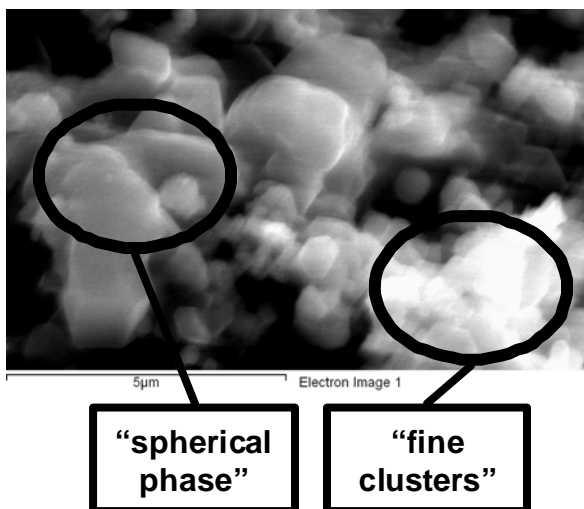


Figure 9. SEM imaging and EDX analysis indicated the presence of an aluminum-rich spherical and sodium rich fine clusters

Discussion

The most significant changes in the sample appear to be morphological. We observed the growth of a shoulder on the higher angle side of the 38.5 degree aluminum peak that has been correlated to the growth of a catalytically inactive Al-Ti alloy. Haiduc et al⁶ determined that Al-Ti alloys are kinetically important. An amorphous phase characterized by a broad reflection of the 38.5 degree peak extending beyond 42 degrees was found to be the most catalytically active. This amorphous phase may be responsible for the slight shifting and broad shoulder of the 38.5 degree peak found in the fresh material XRD spectra for the hydrogenated phase (**Figure 6**) and dehydrogenated phase (**Figure 7**). Haiduc observed a catalytically inactive more ordered Al-Ti intermetallic that formed at a higher temperature that is characterized by a more defined peak centered around 39.2 degrees. Al-Ti alloys have also been suggested by the work of Brinks et al^{7, 8} and Weidenthaler.⁹ The loss of the catalytically active amorphous phase and the formation of this intermetallic may be responsible for sharpening of the 38.5 degree peak and the formation of a distinct feature on the higher angle side of the peak after 100 cycles (see arrows in **Figure 6** and **Figure 7**). It is likely that the majority of the kinetic and apparent capacity degradation experienced during cycling under these conditions is due to the formation of the catalytically inactive Al-Ti alloy.

The SEM and EDX measurements indicate the possible segregation of Ti to the sodium rich clusters where it is less likely to participate catalytically in the reaction. If this is true, it would be

possible to redistribute the titanium from the sodium-rich particles to the remaining aluminum particles thus restoring a portion of the catalytic activity.

The formation of sodium oxides during cycling is also indicated by the evolution of sodium metal at high temperatures during thermal decomposition of the aged sample. It should be noted that only the thermal decomposition of aged materials indicated the presence of these oxides which may be due to the low-level of oxidation present (<5% of the Na). Other components within the aged sample could also include oxygen, but at undetectable levels. It is possible that the formation of low-level sodium oxides could be responsible for hydrogen capacity degradation.

Attempts were made to restore the capacity and kinetics of the cycled sodium alanates through in-situ and ex-situ means. In-situ methods assumed that the changes in the sample were due to crystal growth or agglomeration of the aluminum while at high temperature during desorption. To test this theory, the sample was fully absorbed with hydrogen and then allowed to cool at the absorption pressure of 122 bar. The sample was then decomposed at a very slow rate near 120 °C. Subsequent cycling indicated that this method of in-situ restoration was ineffective.

Subsequent milling of the aged materials resulted in significant success in the restoration of the capacity and kinetics. Milling of 10g of the aged material was performed under the same conditions as utilized during synthesis. Complete restoration was observed for the hexahydride kinetic and capacity performance while nearly complete restoration was observed for the tetrahydride phase as shown in **Table I** and **Figure 2**. It is possible that only the titanium that did not form an intermetallic bond with aluminum, i.e. the titanium found in the sodium clusters, was re-distributed and made catalytically available for the reaction by ball milling. The inability to restore the remaining 0.17 wt% of hydrogen capacity could be due to the partial oxidation of the sodium.

Summary

Titanium-catalyzed sodium alanates show degradation in capacity and kinetics after repeated hydrogen cycling. Analyses of this material show no signs of hydrocarbon contamination. The formation of an intermetallic Ti/Al alloy is likely to be responsible for the hydrogen capacity and kinetic degradation observed. This conclusion is supported by XRD and SEM measurements of the material. A small amount of oxidized sodium in the sample may contribute to capacity degradation as indicated by thermal decomposition analysis. Nearly full restoration of the catalytic activity was observed by re-ballmilling, mostly facilitated by the redistribution of the titanium from the sodium-rich particles to the remaining aluminum particles. The remaining 0.17 wt% of capacity that was not restored may be caused by partial oxidation of sodium.

References

1. B. Bogdanovic, M. Felderhoff, M. Germann, M. Hartel, A. Pommerin, F. Schuth, C. Weidenthaler, B. Zibrowius, *J of Alloys and Compounds*, 350 (2003) 246-255.
2. S. Srinivasan, H. W. Brinks, B. C. Hauback, D. Sun, C. M. Jensen, *J. Alloys and Compounds*, 377 (2004) 283-289.
3. 15. Behrens, R., Jr., *Review of Scientific Instruments*, 1987. 58(3): p. 451-461.
4. D. Dedrick, R. Behrens, R. Bradshaw, *The reactivity of sodium alanates with O₂, H₂O, and CO₂*, Sandia Report, SAND2007-4960.
5. Silverstein, R M and Webster, F X, *Spectrometric Identification of Organic Compounds, Sixth Edition*, John Wiley & Sons, Inc, 1998, Chapter 3, Section 3.6, Pg 82.
6. G. Haiduc, H. A. Stil, M. A. Schwarz, P. Paulus, J. J. C. Geerlings, *J. Alloy and Compounds*, 393 (2005) 252-263.
7. H. W. Brinks, B. C. Hauback, S. S. Srinivasan, C. M. Jensen, *J. Phy. Chem. B* 2005, 109, 15780-15785.
8. H. W. Brinks, C. M. Jensen, S. S. Srinivasan, B. C. Hauback, D. Blanchard, K. Murphy, *J. Alloys and Compounds*, 376 (2004) 215-221.
9. C. Weidenthaler, A. Pommerin, M. Felderhoff, B. Bogdanovic, F. Schuth, *Phys. Chem. Chem. Phys*, 5(2003) 5149-5153.

DISTRIBUTION LIST

GM Research and Development Center

Executive

A. I. Taub (Alan I Taub/US/GM/GMC@GM)

GM Intelligence

B. G. Wicke (Brian G. Wicke/US/GM/GMC@GM)

Chemical & Environmental Sciences Lab

J. A. Spearot (James A. Spearot/US/GM/GMC)
M. P. Balogh (Michael P. Balogh/US/GM/GMC@GM)
M. Cai (Mei Cai/US/GM/GMC@GM)
A. Dailly (anne.dailly@gm.com)
S. W. Jorgensen (scott.w.jorgensen@gm.com)
G. C. Garabedian (Gregory C. Garabedian/US/GM/GMC@GM)
S. Kumar (Sudarshan Kumar/US/GM/GMC@GM)
A. M. Mance (Andrew M. Mance/US/GM/GMC@GM)
G.-A. Nazri (G. Nazri/US/GM/GMC@GM)
S. J. Swarin (Steve Swarin/US/GM/GMC@GM)
C. A. Wong (Curtis A. Wong/US/GM/GMC@GM)
H. Zhang (Hui Zhang/C/US/GM/GMC)
M. Sulic (Martin Sulic/C/US/GM/GMC)

Materials & Processes Lab

M. W. Verbrugge (Mark W. Verbrugge/US/GM/GMC)
J. F. Herbst (Jan F. Herbst/US/GM/GMC@GM)
M. S. Meyer (Martin S. Meyer/US/GM/GMC@GM)
C. H. Oik (Charles H. Oik/US/GM/GMC@GM)
F. E. Pinkerton (Frederick E. Pinkerton/US/GM/GMC@GM)
Q. Hu (Qingyuan Hu/C/US/GM/GMC)
G. Meisner (Gregory P. Meisner/US/GM/GMC)

Fuel Cell Lab

U. Eberle (Ulrich Eberle/DE/OPEL/GMC@GME)
D. Hasenauer (Dieter Hasenauer@GMRUESSELSHEIM)
M. M. Hermann (Michael M Hermann/US/GM/GMC@GM)
J. Meusinger (Josefine Dr Meusinger@GMRUESSELSHEIM)
R. von Helmolt (Rittmar Dr von Helmolt/DE/OPEL/GMC@GME)

HRL Laboratories

J.J. Vajo (vajo@hrl.com)